High-pressure electronic structure and phase transitions in monoclinic InSe: X-ray diffraction, Raman spectroscopy, and density functional theory

D. Errandonea,[1] D. Martínez-García,[1] A. Segura,[1] J. Haines,[2] E. Machado-Charry,[3] E. Canadell,[4] J. C. Chervin,[5] and A. Chevy[5]

[1]*MALTA Consolider Team, Departamento de Física Aplicada-ICMUV, Universitat de València, Edificio de Investigación, c/Dr. Moliner 50, 46100 Burjassot (Valencia), Spain*

[2]*Laboratoire de Physicochimie Matiere Condensee, Université Montpellier 2, CNRS, UMR 5617, F-34095 Montpellier 5, France*

[3]*Institut Català de Nanotecnologia, Campus de la UAB, Edificio C, 08193 Bellaterra, Spain*

[4]*Institut de Ciència de Materials de Barcelona (ICMAB-CSIC), Campus de la UAB, 08193 Bellaterra, Spain*

[5]*IMPMC, Université Pierre et Marie Curie, F-75015 Paris, France*

(Received 22 October 2007; published 22 January 2008)

We have studied the crystal and electronic structure of monoclinic (MC) InSe under pressure finding a reversible phase transition to a Hg_2Cl_2-like tetragonal phase. The pressure evolution of the crystal structure was investigated by angle-dispersive x-ray diffraction and Raman spectroscopy in a diamond-anvil cell up to 30 GPa. From the diffraction experiments, we deduced that MC InSe becomes gradually more symmetric under pressure, transforming the crystal structure into a tetragonal one at 19.4 ± 0.5 GPa. This phase transition occurs without any volume change. Raman measurements under pressure confirmed the occurrence of a monoclinic-to-tetragonal transformation. The nondegenerate modes in the MC phase, especially the A_g^4 modes, exhibit a negative pressure coefficient, converging with the B_g^1 modes, and becoming an *Eg* mode in the tetragonal phase. The experimental results are interpreted through density-functional theory (DFT) electronic-structure and total-energy calculations, which showed that beyond 18 GPa the tetragonal phase is the most stable phase. It is also shown that along the continuous change from monoclinic to tetragonal InSe, there is a progressive decrease of the band gap and eventually, in the tetragonal phase, there occurs a small band overlap. However, the Raman-effect and optical-absorption measurements suggest that this overlap is probably due to the usual DFT band-gap underestimation. Tetragonal InSe is most likely a low-gap semiconductor. The bonding in the monoclinic phase and that in the tetragonal InSe phase are compared.

DOI: 10.1103/PhysRevB.77.045208 PACS number(s): 62.50.−p, 71.20.Nr, 78.40.Fy, 64.70.K−

I. INTRODUCTION

The semiconductor indium selenide (InSe) attracts a great deal of interest because of its optical properties[1,2] and the possibility of preparing high-quality thin films.[3] InSe crystallizes at ambient conditions in a rhombohedral layered phase (InSe-I)—known as γ polytype—which belongs to the space group $R3m$.[4] Its electronic and structural properties have been widely investigated under compression.[2,5–13] In particular, it has been established that at high pressure and room temperature, InSe undergoes a phase transition toward a metallic rocksalt (RS) cubic phase (InSe-III) near 10 GPa.[11,12] In addition, at high pressure and high temperature (HP-HT), the layered γ polytype of InSe transforms into a monoclinic (MC) phase (InSe-II) with space-group symmetry $P2/m$.[9,10] This monoclinic phase can be recovered from HP-HT conditions, remaining metastable at ambient conditions. The monoclinic $P2/m$ structure of InSe [see Fig. 1(a)], which has four molecular units contained in the unit cell, is also a layered structure.[9] It is built up by Se-In-In-Se layers, being differentiated from the γ polytype by the fact that in the $P2/m$ structure, the In-In bonds are parallel to the layers, while in the γ-polytype, they are perpendicular to the layers. The pressure-temperature (P-T) stability range of MC InSe has been recently extensively studied.[9] The pressure effects on the optical properties of MC InSe have been lately investigated too.[9] However, its high-pressure structural behavior has not been studied yet. With the aim of improving the characterization of the high-pressure properties of MC InSe, we report here powder angle-dispersive x-ray diffraction (ADXRD) and Raman spectroscopy measurements of monoclinic InSe under compression up to pressures close to 30 GPa. These results are analyzed under the light of first-principles band-structure calculations. In Sec. II, we will describe the experimental methods and the details of the total-energy and band-structure calculations. In Sec. III, we will present and discuss the results on the structural and lattice dynamical behavior of monoclinic and tetragonal InSe. Their electronic structures will be also discussed there.

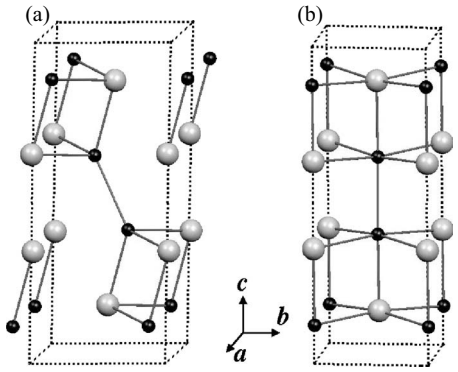

FIG. 1. Schematic view of the crystalline structure of (a) monoclinic InSe and (b) tetragonal InSe. In atoms are shown in black and Se atoms in gray. The first neighbors interatomic bonds are shown.

II. EXPERIMENTAL DETAILS AND THEORETICAL CALCULATION METHODS

A. Experiments

The materials used for the studies were two polycrystalline pieces of MC InSe synthesized using the Bridgman cell described in Ref. 5. In the present case, the heating system of the Bridgman cell was improved by using internal graphite disks as heating elements and molybdenum foils, with very high melting temperatures,[14,15] to apply the electric current to the heaters. By applying a 60 A current, we obtained temperatures higher than 840 K inside the sample pressure chamber. The temperature was measured using a K-type thermocouple and the pressure was determined by the calibration of the applied load.[16–18] Pressure effects on the thermocouple electromotive force were neglected.[19] The conditions of the synthesis were 1 GPa and 700 K and were held for 1 h. The recovered samples were analyzed by Raman spectroscopy and x-ray powder diffraction to unequivocally establish that they corresponded to the monoclinic phase of InSe. For ADXRD experiments, samples were prepared as fine ground powders from the synthesized pieces of MC InSe. For the Raman measurements, a small piece, cleaved from one of the synthesized crystals, was the used sample.

High-pressure angle-dispersive x-ray diffraction experiments were carried out employing zirconium-filtered monochromatic molybdenum radiation (K_α line) from a 800 W fine-focus x-ray tube and using an image plate detector. An x-ray capillary optic was used to focus the x-ray beam giving a beam diameter of 100 μm. ADXRD patterns were obtained on an imaging plate placed at 143.6 mm from the sample. Exposure times were typically of about 48–60 h. A finely powdered sample of monoclinic InSe was compressed using a diamond-anvil cell from 1 bar to 30.5 GPa. The sample was loaded together with sodium chloride (NaCl), which acted as a pressure gauge, and a 4:1 methanol-ethanol mixture, as pressure-transmitting medium, inside a tungsten (W) gasket. We used the equation of state (EOS) of NaCl to determine the pressures.[20,21] We were careful to limit the maximum pressure of our experiments to the pressure stability range of the $B1$ phase of NaCl,[22] since the structural properties of the sample studied may be affected by the large volume collapse that NaCl undergoes at the $B1$-$B2$ phase transition.[22] Determination of peak positions, indexing, structure solution, and refinements of the lattice parameters were performed using the POWDERCELL program.[23]

Raman scattering measurements under pressure were conducted using a membrane diamond-anvil cell (MDAC).[24,25] The studied sample was loaded, along with a ruby microsphere,[26] in an Inconel gasket using neon as pressure-transmitting medium. Neon was charged using the device described in Ref. 27. Pressure was measured by the ruby fluorescence technique.[28] Raman spectra and ruby luminescence were recorded in the backscattering geometry by means of a Jobin-Yvon T64000 Raman spectrometer equipped with a confocal microscope and a liquid N_2-cooled charge coupled device (CCD) detector. The 514.5 nm Ar^+ line was used for Raman excitation, and its plasma peaks were used as fixed frequency references.

B. Theoretical calculation methods

The calculations were carried out using a numerical atomic orbitals density functional theory (DFT) approach.[29] This method is designed for efficient calculations in large systems and implemented in the SIESTA code.[30] We have used the local-density approximation to DFT and, in particular, the functional of Perdew and Zunger.[31] Only the valence electrons are considered in the calculations, with the core being replaced by norm-conserving scalar relativistic pseudopotentials[32] factorized in the Kleinman-Bylander form.[33] Nonlinear partial-core corrections were used to describe the exchange and correlation in the core region.[34] We have used a optimized double-ξ basis set including polarization orbitals for all atoms.[35] The energy cutoff of the real-space integration mesh was 500 Ry. The simulation cells employed have either four (primitive cell) or eight atoms (nonprimitive cell). Thus, the Brillouin zones were sampled using grids of $7\times7\times7$ or $4\times4\times4$ k points, respectively.[36] We checked that the results were well converged with respect to the real-space grid and the Brillouin zone (BZ) sampling.

III. RESULTS AND DISCUSSION

A. Angle dispersive x-ray diffraction under pressure

The *in situ* ADXRD data measured at different pressures are shown in Fig. 2, where NaCl and W peaks are marked. These peaks can be easily identified since their pressure evolution considerable differs from that of the InSe peaks. The rest of the Bragg peaks measured in the diffraction patterns can be indexed with the monoclinic InSe-II structure up to 15.2 GPa (147 reflections at 1 bar). At 1 bar, we found the following lattice parameters: $a=4.092(6)$ Å, $b=4.637(7)$ Å, $c=10.981(9)$ Å, and $\alpha=87.05(3)°$, in good agreement with those previously reported in the literature.[9,10] The independent In [Se] atoms are located at the Wyckoff positions of the $P2/m$ group: $2m$ (0, 0.125, 0.885) and $2n$ (0.5, 0.375, 0.615) [$2m$ (0, 1, 0.654) and $2n$ (0.5, 0.5, 0.846)]. As pressure increases, the monoclinic structure of InSe becomes more symmetric. This is reflected by several facts. In particular, the Bragg peaks located at 1 bar near $2\theta=13.3°$ (110) and 14.8° (004) merge together into only one peak. The same happens with the peaks at $2\theta=14.5°$ (013) and 14.8° ($0\bar{1}3$), at $2\theta=15°$ (112) and 15.4° ($11\bar{2}$), as well as with several peaks located at 1 bar near $2\theta=19.5°$, which merge into a broad peak. In Fig. 2, it can be seen that the (004) peak, depicted by a star, moves under compression much less than the (110) peak, the strongest peak of MC InSe. At 2.9 GPa, the (004) peak overlaps with the strongest NaCl peak. At higher pressures, the separation between the (110) and (004) peaks of MC InSe gradually decreases until they finally merge in only one peak at 19.4 GPa. At this pressure, additional changes are observed in the diffraction pattern, e.g., most of the low angle peaks of monoclinic InSe disappear. The observed changes are fully reversible upon decompression. We attribute these changes to the occurrence of a phase transition in MC InSe. We would like to mention here that we also observed a broadening of all the diffraction peaks beyond 19.4 GPa. We attribute this broadening to nonhydrostatic

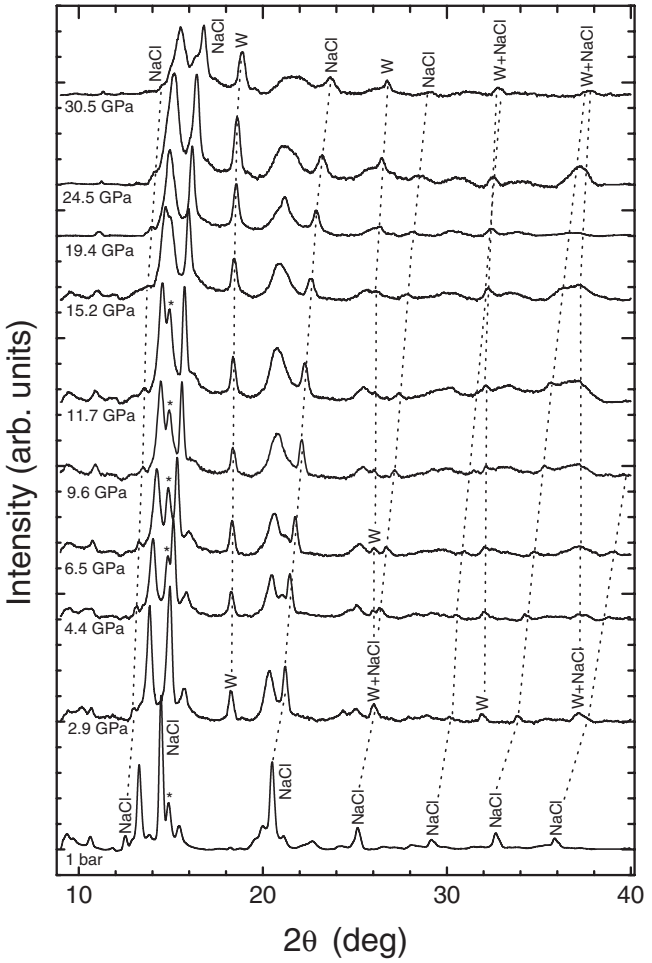

FIG. 2. ADXRD patterns of monoclinic and tetragonal InSe at different pressures. The background was subtracted. NaCl and W peaks are identified. The symbol * indicates the position of the (004) peak of MC InSe.

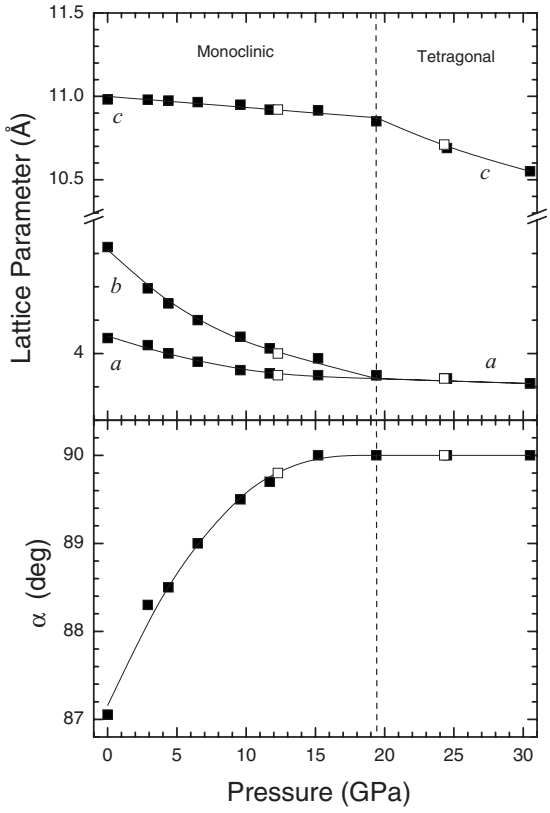

FIG. 3. Pressure evolution of the structural parameters of monoclinic and tetragonal InSe. Solid symbols: pressure increase data. Empty symbols: pressure decrease data. The lines are just a guide to the eye.

stresses probably created due to the use of 4:1 methanol-ethanol as pressure medium.[37]

Background corrected x-ray diffraction (XRD) patterns for all the experiments performed up to 15.2 GPa could be reasonably well fitted with the POWDERCELL program[23] considering the monoclinic InSe-II structure. As we observed preferred orientations effects in our diffraction patterns, we decided not to perform a Rietveld refinement of the high-pressure data and to extract the unit-cell parameters performing a Le Bail analysis.[38] By fitting all the measured patterns up to 15.2 GPa, we obtained the pressure dependences for the lattice parameters of MC InSe, which are illustrated in Fig. 3. There it can be seen that the behavior of MC InSe upon compression is highly anisotropic. While the c parameter is reduced less than 1% from 1 bar to 15.2 GPa, the a and b parameters are reduced 6% and 14%, respectively. In addition, the lattice parameter along the c axis varies almost linearly with pressure, whereas the other two axes exhibit a strong nonlinear dependence on pressure (see Fig. 3). It is important to note here that the covalent In-In bonds of InSe-II form a relatively small angle with the c axis (see Fig. 1). This angle decreases under pressure. The In-In being the strongest bond in InSe-II, and given its tilting under pressure, it is not strange that the c axis of MC InSe is very uncompressible. On the other hand, in Fig. 3, it can also be seen that the monoclinic angle α gradually increases upon compression reaching a 90° value at 15.2 GPa. All these facts confirm that the structure of MC InSe becomes more symmetric upon compression. Indeed, the x-ray diffraction pattern collected at 19.4 GPa can be fitted with the $P2/m$ structure by making $a=b=3.87$ Å, $c=10.85$ Å, and $\alpha=90°$. With these lattice parameters, the monoclinic structure of InSe-II (space group: $P2/m$) is virtually reduced to an orthorhombic structure with space-group symmetry $Pmcm$. However, the patterns collected at 19.4, 24.5, and 30.5 GPa can be best fitted considering a tetragonal structure with space-group symmetry $I4/mmm$ (calomel or Hg_2Cl_2 structure). The consideration of this structure was based upon the results of our theoretical calculations and previous results on the pressure evolution of orthorhombic InS, which has a structure related to that of MC InSe. Concerning the calculations, as we will explain below, the full optimization of the MC InSe structure at ambient pressure by total-energy calculations spontaneously leads to the $I4/mmm$ tetragonal phase. Concerning previous experiments on related compounds, the transition of InS to a Hg_2Cl_2-type structure has been observed to occur at 6 GPa (Ref. 39) but, more recently, Schwarz *et al.*[40] reported a transition of orthorhombic InS to a monoclinic structure at 5 GPa. As InS contains two nonequivalent In-In bonds per

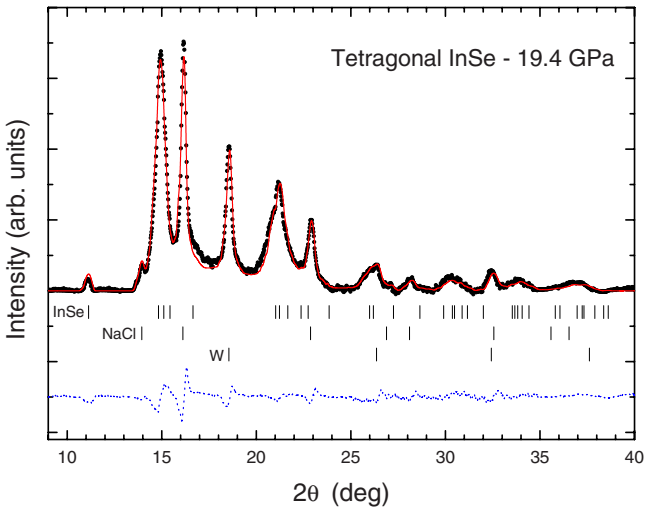

FIG. 4. (Color online) Powder diffraction pattern of tetragonal InSe at 19.4 GPa. Black symbols, observations; solid line (red), refined model; dotted line (blue): residual. The position of the Bragg reflections of InSe, NaCl, and W are indicated.

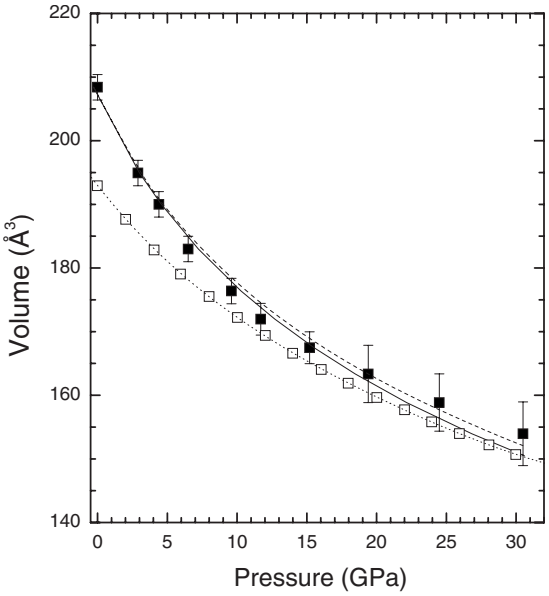

FIG. 5. Pressure dependence of the volume of monoclinic and tetragonal InSe. Solid symbols: experimental data. Empty symbols: theoretical calculations for tetragonal InSe. Solid line: obtained EOS using only the monoclinic InSe data extrapolated up to 30 GPa. Dashed line: obtained EOS using all the data reported. Dotted line: polynomial fit to the theoretical results.

cell, it is plausible that the phase sequence in this compound includes a MC phase similar to InSe II.

Figure 4 shows the fit obtained with the tetragonal structure for the diffraction pattern collected at 19.4 GPa. The lattice parameters obtained from the refinement are $a=b=3.87(1)$ Å and $c=10.85(3)$ Å. The residual of the structural refinement is also shown in Fig. 4. Refinements considering the orthorhombic *Pmcm* structure and cubic RS structure give larger residuals.

It must be noticed that the merging of (110) and (004) XRD peaks into a single one is not a feature of an arbitrary tetragonal structure, but a result of the specific values of the a and c parameters in tetragonal InSe ($c \cong 2\sqrt{2}a$). This seems to be a feature of III-VI compounds with calomel tetragonal structure, as it was also observed for InS.[39] This fact suggests that a RS structure would also, in principle, give account for the XRD peaks positions. Apart from the larger residuals previously mentioned, this possibility can be excluded on the basis of elementary phase-stability considerations, precluding the existence of two phases with the same structure but with different equations of state in the same pressure range. At room temperature layered γ-InSe is known to transit to a well characterized metallic RS phase at 10 GPa.[7,11] If one assumes a RS phase in order to reproduce the XRD peak positions of the sample at 19.4 GPa, the unit-cell parameter must be $a=5.44(1)$ Å. This value differs by more than ten error bars from the a parameter of RS InSe at the same pressure, $a=5.33(1$ Å$)$.[11] Finally, as we will see in the next section, the phase to which MC-InSe transits exhibits four first-order Raman-active modes, while optical phonons in RS InSe have odd parity and are Raman forbidden.[41]

The structure of tetragonal InSe is shown in Fig. 1(b). More details about it will be given when discussing the theoretical results. However, from Fig. 1, it can be already seen that tetragonal InSe is a symmetrized and compressed version of monoclinic InSe obtained basically by a displacement of the In atoms [see Fig. 1(b)]. MC InSe consists basically of 3Se-In-In-3Se chains tilted by about 24° from the c axis. In this structure, at 1 bar pressure, there are one In-Se bond of 2.680 Å, two In-Se bonds of 2.731 Å, and one In-In bond of 2.738 Å. The second next neighbors to each In atom are two additional Se atoms (those at the edge of the unit cell in Fig. 1), with an In-Se bond distance of 3.558 Å. These six bonds form highly distorted octahedra around each In atom. As the In atoms gradually move from their original position under compression, the tilting of the In-In bond with respect to the c axis is reduced, making the structure more symmetric. As a consequence of it, in the tetragonal phase, each In atom is bonded to an In atom and a Se atom, located on top and below it [see Fig. 1(b)]. The In-In and In-Se bond distances are 2.642 and 2.616 Å at 19.4 GPa. In addition to that, the tetragonal phase has also four In-Se bonds of 2.740 Å. These six bonds form a nearly perfect octahedron. In order to close this part of the discussion, it is important to note here that the symmetry center is preserved throughout the transition and that the tetragonal phase of InSe is not a layered structure.

Figure 5 shows the pressure dependence of the volume of the monoclinic and tetragonal phases of InSe. In particular, it can be seen there that tetragonal InSe exhibits a practically linear volume versus pressure dependence. We have analyzed the volume evolution under pressure using a third-order Birch-Murnaghan EOS.[42] From the EOS fit of the data measured up to 15.2 GPa, we determined for MC InSe the cell volume at 1 bar pressure (V_0), the bulk modulus (B_0), and its pressure derivative. Results are shown in Table I together with those of other InSe phases. We obtained for MC InSe $V_0=207(2)$ Å^3, $B_0=44(4)$ GPa, and $B_0'=5(0.5)$. If we include the data corresponding to the tetragonal phase, very similar parameters are determined: $V_0=207(2)$ Å^3, B_0

TABLE I. Equation of state parameters for InSe crystalline phases.

	InSe-I	InSe-II/Tetragonal	InSe-III
V_0 (Å^3)	351[a]	207(2)	191[a]
B_0 (GPa)	36.5(10)[a]	44(4)	51(2)[a]
B_0'	4.1(3)[a]	5.4(5)	4[a]

[a]Reference 11.

=43(9) GPa, and B_0'=5.4(0.5). The obtained EOS indicates that monoclinic and tetragonal InSe are less compressible than InSe-I (B_0=36.5 GPa) (Ref. 11) and more compressible than InSe-III (B_0=51 GPa).[11] This fact is consistent with the increase of the packing efficiency and of the In (Se) coordination following the InSe-I→InSe-II→InSe-III sequence.

B. Raman effect under pressure

MC InSe belongs to the $P2/m$ (C_{2h}) point group. Having four atoms per unit cell, 12 phonon modes are expected. Group theory yields the following irreducible representation at the Brillouin zone for these modes: $4A_g+2B_g+2A_u+4B_u$.[9] Only even modes are Raman active ($4A_g+2B_g$). All these modes are actually observed in MC InSe, and their eigenvectors have been reported in Ref. 9. Let us notice that the assignment shown in Fig. 8 of Ref. 9 contains an error as one should expect that modes B_g (involving nearly pure bond bending) should have lower frequencies than their A_g partners (involving large bond stretching of both intra- and interlayer distances).

Tetragonal InSe belongs to the space group $I4/mmm$ (D_{4h}). It also has four atoms per unit cell and 12 phonon modes whose irreducible representations at the BZ center are $2A_{1g}+2E_g+2A_{2u}+2E_u$. Two of the odd modes ($A_{2u}+E_u$) are the acoustical ones and the other two are the polar optical modes. The even modes are all Raman active. Taking into account compatibility conditions, it is expected that two nondegenerate couples A_g+B_g in MC InSe converge into two doubly degenerate E_g modes in the tetragonal structure (see Fig. 6).

Figure 7 shows the evolution of the Raman spectrum of MC InSe under pressure. Unfortunately, only four modes are clearly resolved at low pressure in the MC-InSe Raman spectra taken inside the MDAC. The two B_g modes are not observed probably because of the sample orientation. The pressure evolution of phonon frequencies is shown in Fig. 8. Table II shows the linear (in both phases) and quadratic (in MC InSe) pressure coefficients of all observed phonon modes, as well as their Grüneisen parameters.

The most striking feature of this pressure evolution is the fact that modes A_g^3 and A_g^4 (involving vibrations perpendicular to the c axis) have very different pressure behavior than modes A_g^1 and A_g^2 (involving vibrations parallel to the c axis). While modes involving vibrations along the c axis exhibit a monotonous pressure dependence, with relatively large and positive pressure coefficients, the pressure evolution of modes involving vibrations perpendicular to the c axis is more complex. In particular, the high-frequency one (A_g^3) is pressure insensitive up to 6–7 GPa, while the low-frequency one (A_g^4) has a negative pressure coefficient up to 10 GPa. Negative pressure coefficients for several phonon modes have also been previously reported in Raman experiments on InS.[43,44]

The pressure evolution of the A_g modes can be explained by the progressive weakening of two In-Se intralayer bonds as coordination changes from the 4+2 one typical of MC InSe to the nearly octahedral six fold coordination of tetrag-

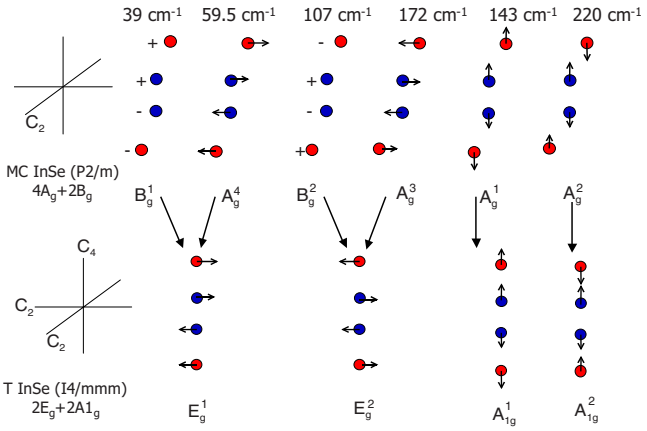

FIG. 6. (Color online) Schematic representation of the Raman-active modes in MC and tetragonal InSe and their expected behavior through the phase transition. Blue (dark) circles, In; red (light) circles, Se.

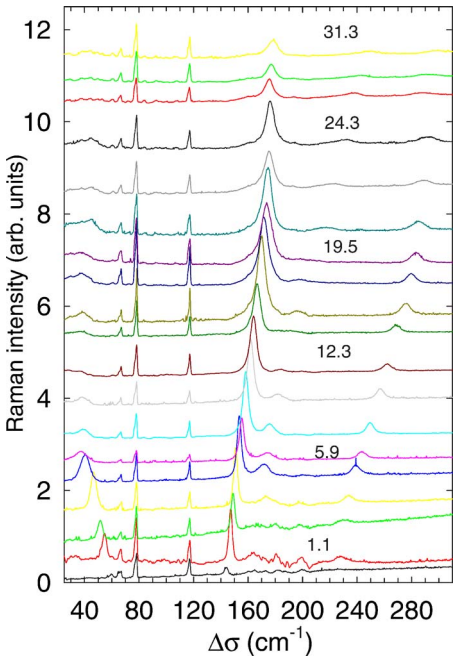

FIG. 7. (Color online) Pressure evolution of the Raman-effect spectra of MC and tetragonal InSe under pressure. The pressure (in GPa) is indicated for some spectra. The peaks observed around 65, 78, and 117 cm^{-1} are plasma lines of Ar$^+$. The feature present around 170 cm^{-1} at low pressure is a CCD artifact.

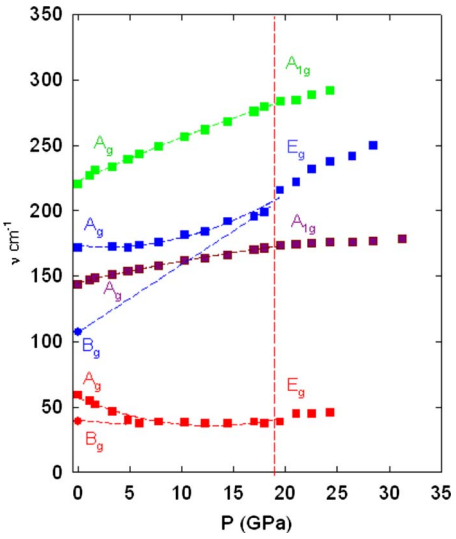

FIG. 8. (Color online) Pressure dependence of the phonon frequencies of Raman-active modes in MC and tetragonal InSe. Different modes are labeled in the figure.

onal InSe [see Fig. 8(b)]. A_g modes mainly involving stretching of covalent In-Se bonds in the *a*-*b* plane [A_g] have small or negative pressure coefficients due the weakening of these In-Se bonds as they evolve from a purely covalent character in MC InSe to a more ionic one in tetragonal InSe. A_g modes involving vibrations along the *c* axis have relatively large pressure coefficients, coherently with the fact that In-Se and In-In bonds parallel to the *c* axis keep their strong covalent character as pressure increases in both the MC and tetragonal phases. At the transition pressure (19.4 GPa), a slope change is observed in the pressure dependence of the phonon frequencies. This change could be accounted for as follows. As MC InSe gets progressively more symmetric under pressure, the *c*-axis change is determined mainly by the compensation of bond-length reduction by bond tilting. The bond stretching character of A_g modes is increased by bond tilting. In the tetragonal phase, no more bond tilting is possible and the frequency change is then determined only by a bond-length reduction.

In Fig. 8, we have also traced lines corresponding to the expected pressure evolution of B_g modes. Given the pressure evolution of the crystal structures, they should converge with the corresponding A_g modes at relatively low pressures when the MC structure is nearly symmetrized.

C. Electronic structure of tetragonal InSe

The layered character of the MC InSe phase precludes any accurate theoretical prediction of its EOS due to the well known inadequacy of DFT for dealing with van der Waals interactions. It is relevant to point out that full optimization of the MC structure spontaneously leads to the tetragonal phase, as the latter can be obtained from the former by a continuous change of the cell parameters and internal coordinates. Significantly, the EOS of the tetragonal phase can be predicted from the fully optimized structures, and the calculated values agree well with the experimental values in the range from 18 to 30 GPa. The calculated (experimental) pressure coefficients for $P > 19$ GPa of the *a* and *c* lattice parameters are −0.0075 (−0.0045) Å/GPa and −0.02 (−0.027) Å/GPa, and the linear variation of the volume with pressure is correctly predicted. A schematic view of the structure obtained in the full optimization is shown in Fig. 9(a). The first observation is that this structure is not a layered structure anymore. Each In atom is bonded to another In atom as in InSe-II. However, now every In atom is also bonded to five Se atoms, four of them lying in the same plane and another in the adjacent plane. Consequently, all In atoms exhibit an octahedral environment with five Se and one In atoms. Thus, we can describe the tetragonal InSe structure as buildup of double layers of the rocksalt InSe structure linked by In-In bonds.

In order to overcome the problem generated by the DFT overestimation of the tetragonal phase stability, the electronic structure of MC InSe at different pressures was calculated by imposing the experimental values of the MC unit-cell parameters and optimizing only the internal atomic coordinates. At ambient pressure, electronic-structure calculations correctly predict that MC InSe is an indirect semiconductor (see Fig. 10) but underestimate its band gap by nearly 1 eV.[9] As pressure increases, band-structure calculations predict a decrease of the band gap. At about 5 GPa, the system becomes a semimetal and then a metal with a 0.8 eV band overlap. However, in these constrained calculations, the relaxed structure at around 5 GPa has already the topology of the tetrag-

TABLE II. Mode frequencies, pressure coefficients, and Grüneisen parameters for phonon modes in monoclinic and tetragonal InSe.

Monoclinic InSe					Tetragonal InSe			
Mode	ω_{iAP} (cm^{-1})	$\left(\frac{d\omega_i}{dP}\right)_{AP}$ (cm^{-1} GPa^{-1})	$\left(\frac{d^2\omega_i}{dP^2}\right)_{AP}$ (cm^{-1} GPa^{-2})	γ_i	Mode	$\omega_{i19\ \mathrm{GPa}}$ (cm^{-1})	$\left(\frac{d\omega_i}{dP}\right)_{19\ \mathrm{GPa}}$ (cm^{-1} GPa^{-1})	γ_i^{a} (19 GPa)
A_g^1	59.5	−3.4	0.13	−2.6(3)	E_g^1	40.4	1.4	5.2(5)
A_g^2	145.1	1.8	−0.02	0.55(5)	A_{1g}^1	173.0	0.38	0.33(3)
A_g^3	172	−0.7	0.13	−0.18(2)	E_g^2	217.0	3.6	2.5(3)
A_g^4	220.5	3.6	−0.02	0.72(7)	A_{1g}^2	283.0	1.7	0.9(1)

[a]Grüneisen parameters in the tetragonal phase have been determined using the bulk modulus at 19 GPa.

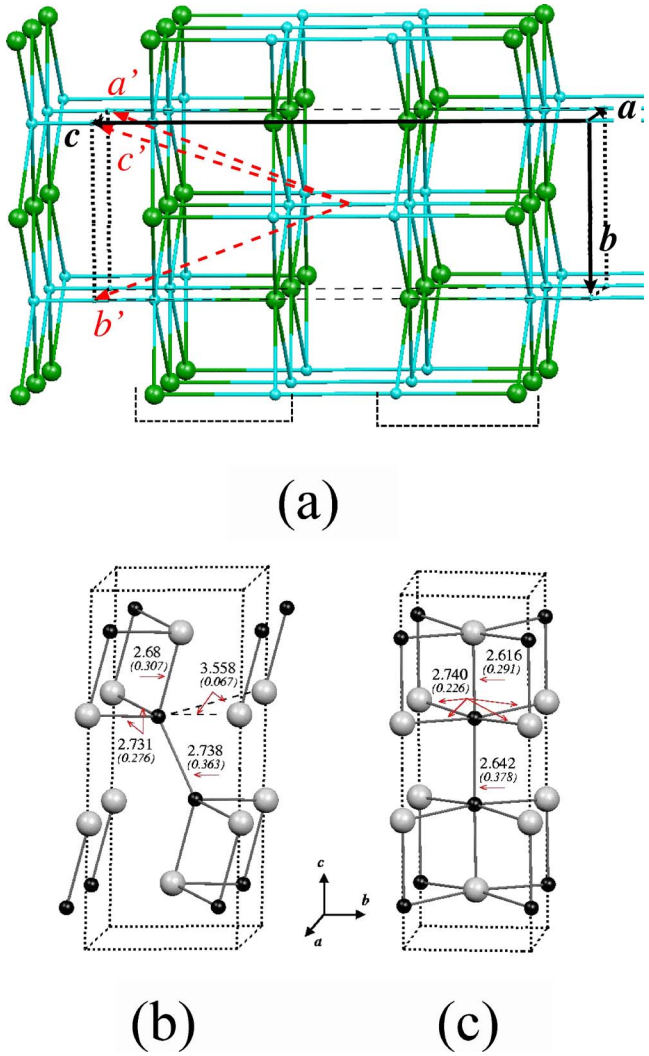

FIG. 9. (Color online) (a) Perspective view of the structure of tetragonal InSe. The In and Se atoms are represented as small (blue) and large (green) spheres, respectively. Schematic view of the (b) monoclinic and (c) tetragonal structures where the calculated In-In and In-Se distances (Å) as well as the associated Mulliken overlap populations are shown. The structures are those of the optimized structures with fixed-cell parameters corresponding to ambient pressure (monoclinic phase) and 19.4 GPa (tetragonal phase).

onal phase. Thus, it is reasonable to assume that along the real transformation, there should be a continuous decrease of the band gap although more gradual than predicted by these calculations. The calculated band structure at 19.4 GPa is shown in Fig. 11. In this diagram, the Γ-*M* line corresponds to the reciprocal-space projection of a direction parallel to the In-In bonds and therefore perpendicular to the double rocksalt layers. The similarity between the Brillouin zones of the monoclinic and tetragonal structures (see Figs. 10 and 11) allows a direct comparison of the two band structures. In fact, most of the bands in the two systems can be correlated since the general shape is kept for most lines. As expected, the close structural relationship between the two structures is also associated with a clear relationship between the electronic structures. However, the band dispersions are larger in

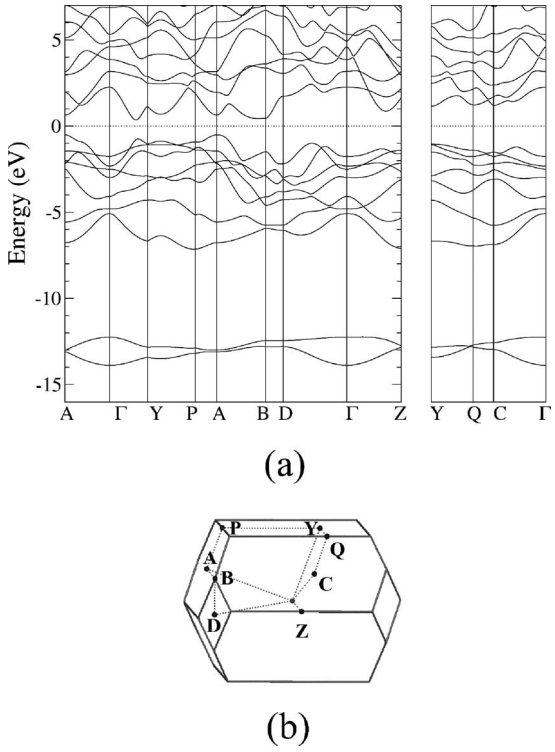

FIG. 10. (a) Calculated band structure of monoclinic InSe at ambient pressure. The structure was optimized using fixed-cell parameters corresponding to ambient pressure. (b) Brillouin zone of monoclinic InSe

the tetragonal structure as a result of the greater delocalization inherent to the rocksalt layers, and the gap disappears, so that tetragonal InSe is predicted to be a metal. Nevertheless, if the DFT band-gap underestimation (around 1 eV at ambient pressure) was maintained upon compression (which is quite likely, given the fact that DFT calculations correctly predict the band-gap pressure coefficients[2]), tetragonal InSe would rather be a semiconductor with a small band gap (around 0.3 eV). This is coherent with both optical and Raman-effect results. No trace of a band-gap closing was observed in the optical-absorption experiments performed up to 16 GPa and reported in Ref. 9. In fact, as the MC-InSe sample used in Ref. 9 was very thin (about 1 μm), only a very intense direct transition at 1.5 eV was observed but the sample remained transparent to infrared light up to 16 GPa. A band-overlap increasing with pressure up to 0.8 eV would have resulted in a free-carrier absorption edge moving quickly to higher energies in the near infrared and turning the sample opaque to infrared light. On the other side, in the Raman results reported here, no discontinuity is observed in the phonon intensities as the sample goes trough the MC-to-tetragonal phase transition. Metallization would necessarily induce a clear reduction of these intensities.

It is interesting to compare the structure and bonding in the two phases [see Figs. 9(b) and 9(c)]. All the data discussed in this section correspond to the optimized structures with fixed experimental cell parameters at 0 GPa (monoclinic) and 19.4 GPa (tetragonal). In the monoclinic phase, the In atoms are involved in three In-Se bonds with distances

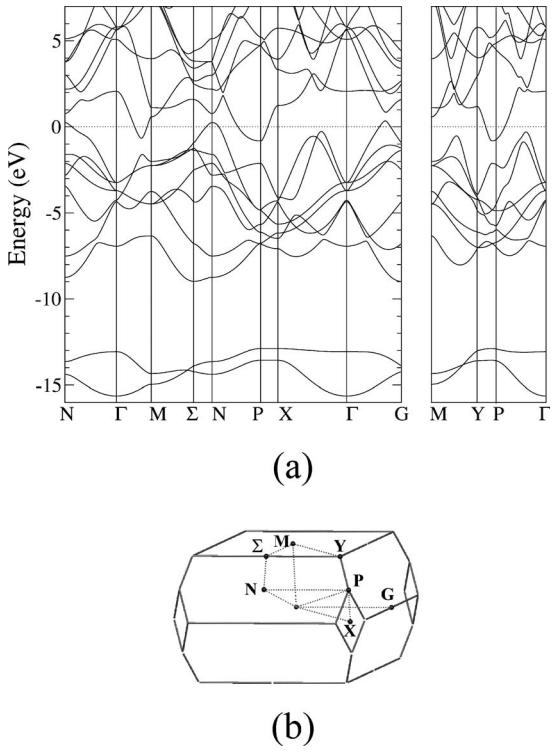

FIG. 11. (a) Calculated band structure of tetragonal InSe at 19.4 GPa. The structure was optimized using fixed-cell parameters corresponding to 19.4 GPa. (b) Brillouin zone of tetragonal InSe.

2.680, 2.731, and 2.731 Å and one In-In bond of 2.738 Å. In addition, two Se atoms of the nearest layer are at 3.558 Å, and these are the two Se atoms which will become bonded to the In atom to complete the octahedral coordination. In the tetrahedral structure, the apical In-Se distance is 2.616 Å, the four basal In-Se distances are 2.740 Å, and the In-In distance is 2.642 Å. Thus, in the monoclinic-to-tetrahedral transformation, the In-In distance shortens, two of the already existing In-Se bonds slightly lengthen, one of the already existing In-Se bonds shortens, and two new In-Se bonds are created. In order to compare the bonding, it is useful to look at the calculated Mulliken overlap populations[45] associated with the different pairs of interacting atoms. Despite its well known shortcomings, these overlap populations provide a useful measure of the strength of a given type of bond in different structures. The calculated overlap populations for the In-In bonds and the three In-Se bonds in the monoclinic structure are 0.363, 0.276, 0.276, and 0.307, respectively [see Fig. 9(b)]. It is very interesting to note that the overlap populations associated with the two Se atoms which will become bonded in the tetragonal structure are positive and far from negligible (0.067 for each of the interactions). This means that the MC structure is very well prepared, both structurally and electronically, to evolve toward the tetragonal structure and that the interlayer interactions are very strong. In the tetragonal structure, the In-In, apical In-Se, and basal In-Se overlap populations are 0.378, 0.291, and 0.226, respectively [see Fig. 9(c)]. Thus, the total overlap population implicating one In atom is 0.993 in the monoclinic structure and 1.195 in the tetragonal structure. It is clear that along the monoclinic-to-tetragonal transformation, there is a slight reinforcement of the In-In bonds (from 0.363 to 0.378) and a decrease of the strength of the already existing In-Se bonds (from 0.859 to 0.743 per In atom), which is more than compensated by the reinforcement of the In-Se bonding associated with the two new In-Se bonds (from 0.134 to 0.452). The tetrahedral structure is favored in terms of both the covalent bonding and Coulomb interactions (the charges are larger and more favorably distributed in the tetragonal structure). Thus, we conclude that the stability of the monoclinic structure must be associated with strong favorable interlayer interactions which are underestimated in our DFT calculations.

It is also interesting to notice that total-energy calculations predict the tetragonal phase to be more stable than the RS one at all explored pressures. Since both structures are three-dimensional and very similar, DFT should correctly predict the relative stability of the two structures. The greater stability of the tetragonal phase can be reasonably attributed to the existence of strong In-In covalent bonds along the *c* axis in between the RS double planes. Experimentally, both phases appear to be stable between 20 and 30 GPa and no transition has been observed between them. Once the RS phase (tetragonal) is attained from rhombohedral (monoclinic) InSe, further heating of the sample does not induce a transition to the tetragonal (RS) phase. This suggest the existence of a very large kinetic barrier between both phases,[46] probably due to the very different atom sequence along the *c* axis (In-Se-In-Se in RS InSe versus In-In-Se-Se in tetragonal InSe).

IV. CONCLUSIONS

Based on XRD and Raman-effect experiments under pressure and DFT calculations, we have shown that monoclinic InSe undergoes a reversible phase transition to a calomel tetragonal phase with symmetry $I4/mmm$. This phase exists at room temperature, in a pressure range through which a previously characterized rocksalt phase is also known to be stable. Total-energy calculations predict that the tetragonal phase should be thermodynamically more stable than the rocksalt one, but a transition between them has never been observed. Electronic-structure calculations predict a metallic character for tetragonal InSe. However, this result is most likely a consequence of the DFT band-gap underestimation as optical and Raman-effect results do not yield any evidence of metallization.

ACKNOWLEDGMENTS

This study was supported by the MEC of Spain (Grants No. MAT2007-65990-C03-01 and No. FIS2006-12117-C04-01), by the Consolider Program (Grants No. CSD2007-00041 and CSD2007-00045), by the Generalitat Valenciana (ACOMP06/181), and by the Generalitat de Catalunya (2005 SGR 683). One of the authors (D.E.) acknowledges the financial support from the MEC and the University of Valencia through the "Ramón y Cajal" program.

[1] Ch. Ferrer-Roca, J. Bouvier, A. Segura, M. V. Andres, and V. Muñoz, J. Appl. Phys. **85**, 3780 (1999), and references therein.
[2] F. J. Manjón, D. Errandonea, A. Segura, V. Muñoz, G. Tobias, P. Ordejon, and E. Canadell, Phys. Rev. B **63**, 125330 (2001), and references therein.
[3] J. F. Sanchez-Royo, A. Segura, O. Lang, E. Schaar, C. Pettenkofer, W. Jaegermann, L. Roa, and A. Chevy, J. Appl. Phys. **90**, 2818 (2001), and references therein.
[4] A. Likforman, D. Carre, J. Etienne, and B. Bachet, Acta Crystallogr., Sect. B: Struct. Crystallogr. Cryst. Chem. **31**, 1252 (1975).
[5] D. Errandonea, A. Segura, F. J. Manjón, and A. Chevy, Semicond. Sci. Technol. **18**, 241 (2003).
[6] A. R. Goñi, A. Cantarero, U. Schwarz, K. Syassen, and A. Chevy, Phys. Rev. B **45**, 4221 (1992).
[7] D. Errandonea, A. Segura, J. F. Sánchez-Royo, V. Muñoz, P. Grima, A. Chevy, and C. Ulrich, Phys. Rev. B **55**, 16217 (1997).
[8] D. Errandonea, A. Segura, F. J. Manjón, A. Chevy, E. Machado, G. Tobias, P. Ordejon, and E. Canadell, Phys. Rev. B **71**, 125206 (2005), and references therein.
[9] D. Errandonea, D. Martínez-García, A. Segura, A. Chevy, G. Tobias, E. Canadell, and P. Ordejon, Phys. Rev. B **73**, 235202 (2006).
[10] H. Iwasaki, Y. Watanabe, N. Kuroda, and Y. Nishina, Physica B & C **105B**, 314 (1981).
[11] U. Schwarz, A. R. Goñi, K. Syassen, A. Cantarero, and A. Chevy, High Press. Res. **8**, 396 (1991).
[12] F. J. Manjon, D. Errandonea, A. Segura, J. C. Chervin, and V. Muñoz, High Press. Res. **22**, 261 (2002).
[13] J. F. Sanchez-Royo, D. Errandonea, A. Segura, L. Roa, and A. Chevy, J. Appl. Phys. **83**, 4750 (1998).
[14] D. Errandonea, B. Schwager, R. Ditz, C. Gessmann, R. Boehler, and M. Ross, Phys. Rev. B **63**, 132104 (2001).
[15] D. Errandonea, Physica B **357**, 356 (2005).
[16] A. K. Bandyopadhya, S. Chatterjee, E. S. R. Gopal, and S. V. Subramanyam, Rev. Sci. Instrum. **32**, 1232 (1981).
[17] M. Nishikawa and S. Akimoto, High Temp. - High Press. **3**, 161 (1971).
[18] D. Errandonea, D. Martínez-García, J. Ruiz-Fuertes, R. Lacomba-Perales, A. Segura, A. Chevy, and L. Roa, High Press. Res. **26**, 513 (2006).
[19] F. P. Bundy, J. Appl. Phys. **32**, 483 (1961).
[20] F. Birch, J. Geophys. Res. **91**, 4949 (1986).
[21] D. L. Heinz and R. Jeanloz, Phys. Rev. B **30**, 6045 (1984).
[22] Y. LePage and P. Saxe, Phys. Rev. B **65**, 104104 (2002).
[23] W. Kraus and G. Nolze, J. Appl. Crystallogr. **29**, 301 (1996).
[24] R. Le Toullec, J. P. Pinceaux, and P. Loubeyre, High Press. Res. **1**, 77 (1988).
[25] J. C. Chervin, B. Canny, J. M. Besson, and P. Pruzan, Rev. Sci. Instrum. **66**, 2595 (1995).
[26] J. C. Chervin, B. Canny, and M. Mancinelli, High Press. Res. **21**, 305 (1992).
[27] B. Couzinet, N. Dahan, G. Hamel, and J. C. Chervin, High Press. Res. **23**, 409 (2003).
[28] H. K. Mao, J. Xu, and P. M. Bell, J. Geophys. Res. **91**, 4673 (1986).
[29] P. Hohenberg and W. Kohn, Phys. Rev. **136**, 864 (1964); W. Kohn and L. J. Sham, *ibid.* **140**, 1133 (1965).
[30] J. M. Soler, E. Artacho, J. D. Gale, A. García, J. Junquera, P. Ordejón, and D. Sánchez-Portal, J. Phys.: Condens. Matter **14**, 2745 (2002).
[31] J. P. Perdew and A. Zunger, Phys. Rev. B **23**, 5048 (1981).
[32] N. Troullier and J. L. Martins, Phys. Rev. B **43**, 1993 (1991).
[33] L. Kleinman and D. M. Bylander, Phys. Rev. Lett. **48**, 1425 (1982).
[34] S. G. Louie, S. Froyen, and M. L. Cohen, Phys. Rev. B **26**, 1738 (1982).
[35] E. Anglada, J. M. Soler, J. Junquera, and E. Artacho, Phys. Rev. B **66**, 205101 (2002).
[36] H. J. Monkhorst and J. D. Pack, Phys. Rev. B **13**, 5188 (1976).
[37] D. Errandonea, Y. Meng, M. Somayazulu, and D. Häusermann, Physica B **355**, 116 (2005).
[38] A. Le Bail, H. Duroy, and J. L. Fourquet, Mater. Res. Bull. **23**, 447 (1988).
[39] S. S. Kabalkina, V. G. Losev, and N. M. Gasalny, Solid State Commun. **44**, 1383 (1982).
[40] U. Schwarz, H. Hillebrecht, and K. Syassen, Z. Kristallogr. **210**, 494 (1995).
[41] C. Ulrich, M. A. Mroginski, A. Goñi, A. Cantarero, U. Schwarz, V. Muñoz, and K. Syassen, Phys. Status Solidi B **198**, 121 (1996).
[42] F. Birch, J. Geophys. Res. **83**, 1257 (1978).
[43] F. E. Fardzhev, N. M. Gasalny, A. S. Ragimov, A. F. Goncharov, and S. I. Subbotin, Solid State Commun. **39**, 587 (1981).
[44] U. Schwarz, H. Hillebrecht, A. Goncharov, and K. Syassen, Zeitschrift fur Kristallographie Supplement Series **9**, 44 (1995).
[45] R. S. Mulliken, J. Chem. Phys. **23**, 1833 (1955).
[46] D. Errandonea, J. Pellicer-Porres, F. J. Manjón, A. Segura, Ch. Ferrer-Roca, R. S. Kumar, O. Tschauner, J. López-Solano, P. Rodríguez-Hernández, S. Radescu, A. Mujica, A. Muñoz, and G. Aquilanti, Phys. Rev. B **73**, 224103 (2006).